

1 Article

2 **High gas hydrate and free gas concentrations: an** 3 **explanation for seeps offshore south Mocha Island**

4 Iván Vargas-Cordero ^{1,*}, Umberta Tinivella ², Lucía Villar-Muñoz ³ and Joaquim P. Bento ⁴

5 ¹ Universidad Andres Bello (UNAB), Facultad de Ingeniería, Viña del Mar, Chile; ivan.vargas@unab.cl

6 ² Istituto Nazionale di Oceanografia e di Geofisica Sperimentale (OGS), Trieste, Italy; utinivella@inogs.it

7 ³ Helmholtz Centre for Ocean Research (GEOMAR), Kiel, Germany; lucia.villar@gmail.com

8 ⁴ Escuela de Ciencias del Mar, Pontificia Universidad Católica de Valparaíso, Valparaíso, Chile;

9 jnettojunior@gmail.com

10 * Correspondence: ivan.vargas@unab.cl; Tel.: +56-950598066

11 Received: date; Accepted: date; Published: date

12 **Abstract:** Recent studies have reported shallow and deep seep areas offshore Mocha island. Gas
13 hydrate occurrences along the Chilean margin could explain seeps presence. Gas phases (gas
14 hydrate and free gas) and geothermal gradients were estimated analysing two seismic sections.
15 Close to Mocha island (up to 20 km) were detected high (up to 1900 m/s) and low (1260 m/s)
16 velocities associated with high gas hydrate (up to 20 % of total volume) and free gas (up to 1.1% of
17 total volume) concentrations respectively. These values are in agreement with a variable and high
18 geothermal gradient (65 to 110 °C/km) related to high supply deep fluids canalised by faults and
19 fractures. Faraway from Mocha island (more than 60 km), free gas concentrations decrease to 0.3 %
20 of total volume and low geothermal gradient (from 35 to 60 °C/km) are associated with low fluids
21 supply. Finally, we propose gas hydrate dissociation processes as the main supply source for seeps
22 in the vicinity of Mocha island. These processes can be triggered by ancient sliding reported in
23 literature.

24 **Keywords:** gas hydrate; BSR; Mocha island

25

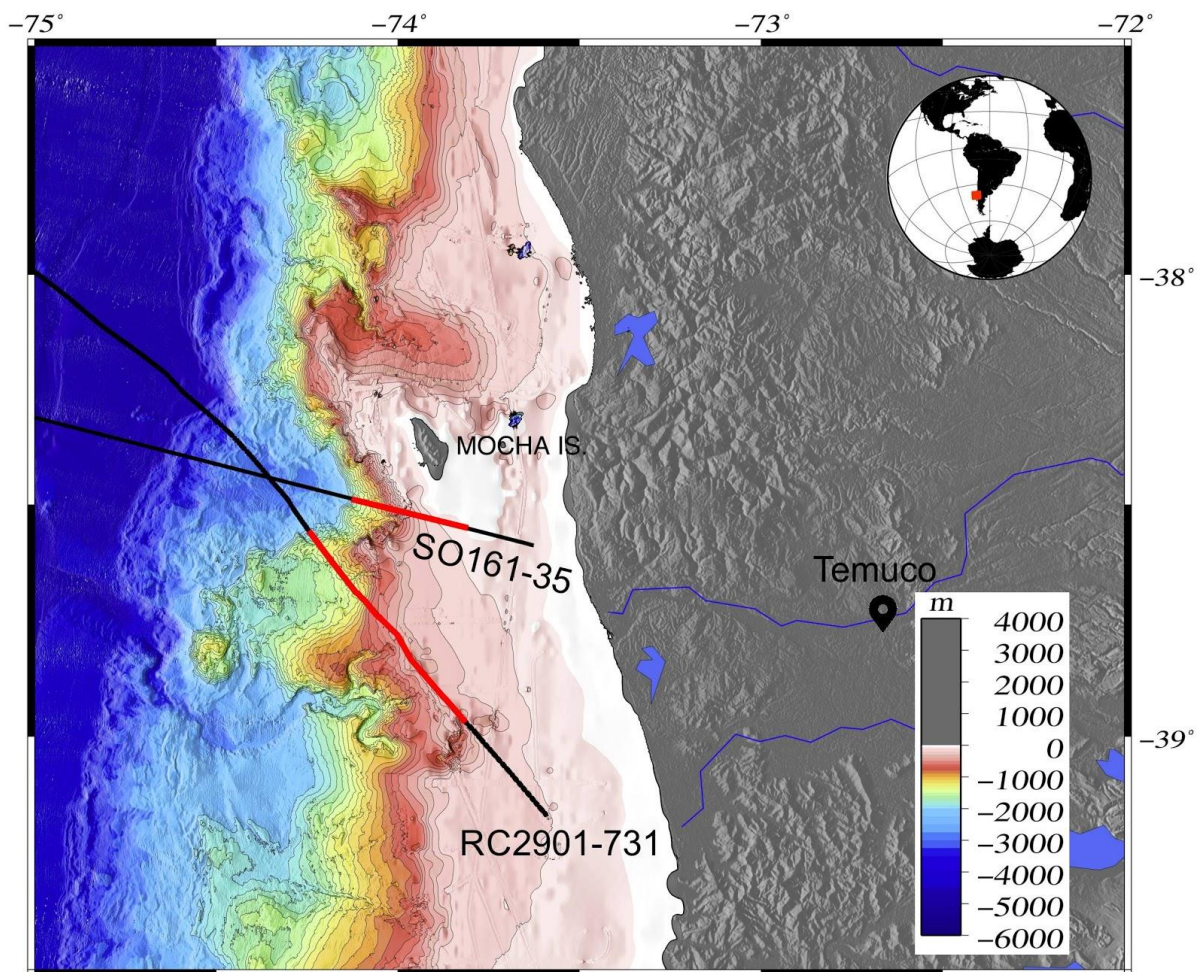
26 **1. Introduction**

27 The studies regarding gas hydrate occurrences worldwide are important for three main reasons:
28 a) energy resource; b) submarine geohazard and c) global climate change [1]. Gas hydrate distribution
29 has been mapped mostly by using indirect measurements. From multichannel seismic data, it is
30 possible to detect the principal indicator of gas hydrate presence known as bottom simulating
31 reflector (BSR). The worldwide distribution of BSR occurs mainly in marine sediments along the
32 active continental margins (predominantly circum-Pacific belt) and the permafrost regions
33 (Antarctic and Arctic).

34 In Chile the interest for gas hydrate occurrences plays an important role due to the high
35 seismicity that characterises the entire region. Several scientific studies have reported gas hydrate
36 dissociation triggered by earthquakes e.g. Great Sumatra, Japan and Norwegian margins [2-6]. The
37 BSR along the Chilean margin is recognized in the continental slope covering a wide extension close
38 to 3000 km (from 33°S until 56°S). In this context, gas hydrate estimates contribute to evaluate
39 submarine geohazards associated with gas hydrate dissociation and the potential methane reservoir.
40 Moreover, the estimates of methane stored as gas hydrate and free gas phases in marine sediments
41 can be used to model more realistic scenarios associated with gas hydrates dissociation and its effects
42 as a greenhouse gas. Several studies along the Chilean margin have reported gas phases
43 concentrations by modelling the seismic velocity [7-16] covering already 10% of the entire margin.

44 The present study add new information regarding gas phase concentrations southernwards
 45 offshore Mocha Island by using seismic and theoretical velocity models (Fig. 1). The Mocha island is
 46 characterised by active seismicity and constitutes an uplifted block during the Quaternary and
 47 emerged today in the Arauco peninsula [17,18]. Moreover, Mocha island is known by intertidal and
 48 subtidal gas seepage system [19,20] and deeper seeps at 1400 water depth [21], whose presence
 49 probably is related to gas hydrates dissociation. In this context, gas phases estimates contribute to
 50 map and understand its role in fluid escapes supply.

51 In order to quantify gas phases a procedure already tested in previous studies is performed [11-
 52 16,22]. The method includes: a) Obtaining seismic velocity model by using Kirchhoff Pre-Stack Depth
 53 Migration (PSDM); b) Velocity anomalies evaluation; c) Gas phases estimates by fitting seismic
 54 velocity with theoretical velocity and d) Geothermal gradient calculation by using seafloor and BSR
 55 depths and water bottom temperature.



56

57 **Figure 1.** Location map. Red lines indicate the parts of the seismic sections analysed in this study.

58 2. Materials and Methods

59 2.1. Seismic Data

60 RC2901-731 and SO161-35 seismic lines were analysed. Seismic data were acquired during 1988
 61 and 2001 in the framework of ODP (Mid-Ocean Spreading Ridge, Chile Ridge; RC2901-731 seismic
 62 line) and SPOC (Subduction Processes off Chile; SO161-35 seismic line) projects, respectively. Seismic
 63 acquisition parameters are detailed in Table 1. Open-source Seismic Unix [23] software was used to
 64 perform the seismic processing.

65

66

Table 1: seismic acquisition parameters

Seismic lines	Research Vessel	Long streamer	Channels	Intertrace	Shot spacing	Airguns/total volume
RC2901-731	RV/Conrad	3000 m	240	12.5 m	50 m	10/61.3 L
SO161-35	RV/Sonne	3000 m	25 108	12.5 m 25 m	50 m	20/54.1 L

67 *2.2. Inversion Modelling*

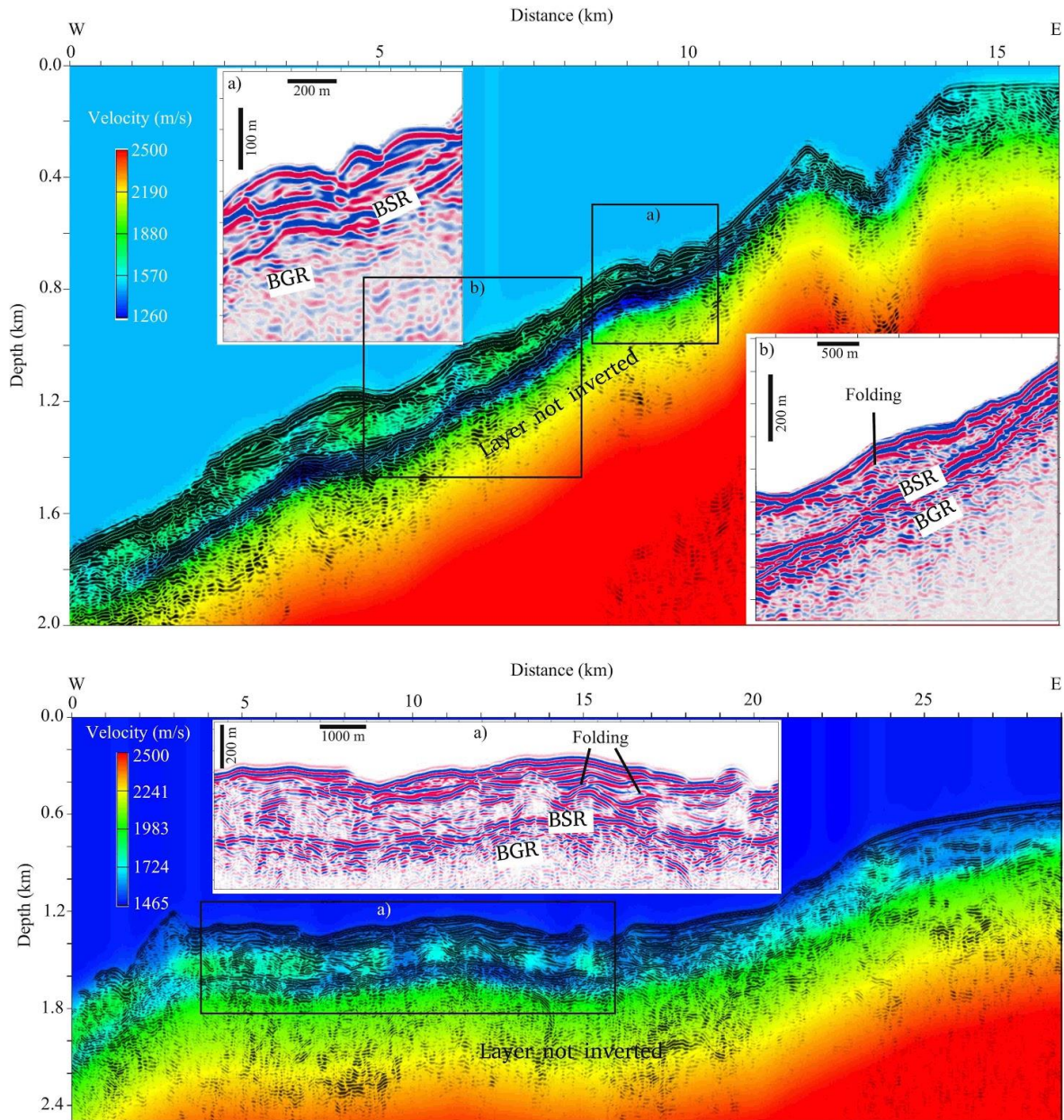
68 Once identified the BSR along seismic lines, two sections close to 20 km-long were chosen. The
69 seismic analysis uses pre-stack data to perform Kirchhoff depth migration in order to model
70 migration velocity by using an iterative algorithm [24]. The seismic migration analysis builds
71 iteratively the velocity model by using a layer stripping approach [25], in which each layer is
72 modelled in depth. The velocity model is built by selecting continuous reflectors. In our case the
73 seafloor (SF), the horizon 1 (H1), the BSR and the base of the free gas (BGR) were selected. The grid
74 was defined considering a vertical and horizontal spacing equal to 10 and 25 m for RC2901-731 and
75 SO161-35 seismic sections, respectively. The migration velocity analysis uses the output of PSDM to
76 evaluate the reliability of velocity by measuring the flatness in Common Image Gathers (CIGs). At
77 each iteration, the migration velocity analysis is corrected for the purpose of to flat the events in the
78 CIGs; when the events became flats, the velocity layer is fixed and a new horizon is analysed. The
79 number of iterations of each layer necessary to flat the events are detailed in Table 2:

80

Table 2: Layer iteration numbers

RC2901-731 seismic section		SO161-35 seismic section	
Layers	Iterations	Layers	Iterations
Seawater	3	Seawater	4
From SF to H1	5	From SF to BSR	15
From H1 to BSR	18	Free gas	10
Free gas	4	-	-

81 A velocity gradient was introduced below the BGR and the final velocity models were smoothed
82 in order to improve the stacked depth migrated image. The stacking of the CIGs was performed by
83 using a maximum offset of 2500 m in order to attenuate stretching effects. Finally, a mixing and band-
84 pass filter was applied; the final sections are shown in Fig. 2.



85

86 **Figure 2.** Pre-stack depth sections with superimposed velocity models. Top: SO161-35 seismic section.
 87 Bottom: RC2901-731 seismic section. Black boxes indicated with letters show the blow-ups.

88 *2.3 BSR-Derived Geothermal Gradient*

89 It is possible to calculate the geothermal gradient (dT/dZ) by using BSR information, as reported
 90 in literature [15,16]. The main parameters to consider are: 1) BSR depth (Z_{BSR}), 2) seafloor depth
 91 (Z_{SEA}), 3) BSR temperature (T_{BSR}) and seafloor temperature (T_{SEA}). Thus the geothermal gradient can
 92 be obtained by using the following relationship:

93
$$dT/dZ = (T_{BSR} - T_{SEA}) / (Z_{BSR} - Z_{SEA})$$

94 where T_{SEA} was obtained from ODP information and reported studies in Central Chile [26,27].
 95 The T_{BSR} is based on gas hydrate stability curves reported by [28]. Finally, Z_{BSR} and Z_{SEA} were taken
 96 from seismic data analysis.
 97

98 2.4 Gas phase concentrations

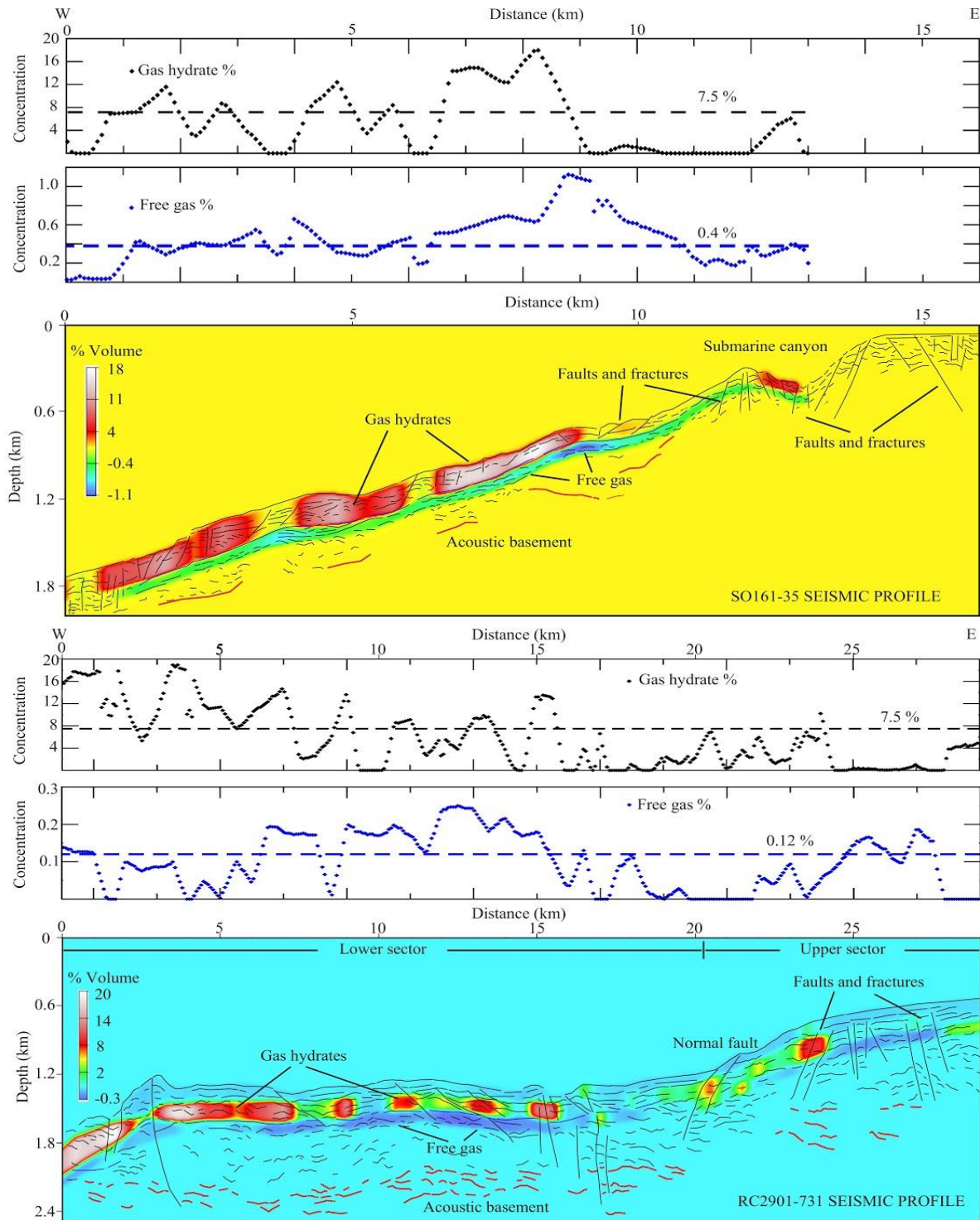
99 Gas phases (gas hydrates and free gas) concentrations are estimated by using a simplified
100 method [29-31] of the Biot theory [30]. The velocity anomalies (i.e., the difference between the
101 background and seismic velocities) are evaluated considering the geological context in order to
102 associate positive velocity anomalies with gas hydrate concentrations and negative velocity
103 anomalies with free gas concentrations. A qualitative estimate can be obtained by comparing
104 theoretical velocity curves in absence of gas (i.e., the background velocity; [32, 33]) with our seismic
105 velocity curves obtained as described in the section 2.2. The method calculates the free gas
106 concentration in the pore space by considering uniform (gas and water in pore space) and patchy (all
107 gas in patches without water) distributions. In our case, an uniform distribution was considered [30].
108 Theoretical velocity was modeled by supposing a porosity at the seafloor of 65%, as measured during
109 ODP leg 202 and reported in [27].

110 3. Results

111 BSRs were recognized in both seismic sections. Along the whole SO161-35 seismic section the
112 BSR is continuous, strong and shows a variable depth reaching maximum thickness in deepest areas
113 (up to 200 m below seafloor -mbsf; see from 0 to 6 km of distance in Fig. 2), while minimum thickness
114 are located in correspondence to shallowest areas (80 mbsf). On the contrary, RC2901-731 seismic
115 profile shows discontinuous and locally strong BSR, while a constant BSR depths of about 250 mbsf
116 are evidenced from 4 to 16 km of distance (Fig. 2). Note that in this section from 16 to 25 km of
117 distance, the BSR is weak or disappear (Fig. 2). In both sections, the BGR is detected and it is
118 characterized by an average thickness of about 70 m (see blow-up in Fig. 2).

119 The velocity distribution across SO161-35 and RC2901-731 sections shows strong vertical and
120 lateral variations. The vertical velocity distribution across SO161-35 and RC2901-731 shows a drop
121 below the BSR reaching minimum values of 1260 m/s and 1465 m/s respectively that can be associated
122 to the free gas presence (see Fig. 2). Regarding lateral velocity variations, high velocity values
123 (ranging from 1700 m/s to 1900 m/s) were recognized above the BSRs (Fig. 2). In both sections, faults
124 and fractures with small slips affecting the seafloor were identified in correspondence to low velocity
125 values (Fig. 3). Moreover, in the eastern part of the SO161-35 section a submarine canyon was
126 identified (Fig. 2 and Fig. 3) and a normal fault that configures a lower and upper sector of the
127 RC2901-731 line (see bottom panel of Fig. 3 at 22 km of distance). Finally, in both sections locally
128 dipping reflections were associated to folding (see blow-ups in Fig. 2).

129 Variable gas hydrate and free gas concentrations were identified, even if the gas hydrate average
130 concentrations are equal to 7.5% of total volume in both sections. On the contrary, the free gas average
131 concentrations are different and equal to 0.4% and 0.12% of total volume in the SO161-35 and RC2901-
132 731 sections respectively. An opposite gas phase concentration trend was observed, in which high
133 gas hydrate concentrations (ranging from 12% to 20% of total volume) overlies to low free gas
134 concentrations (< 0.4% of total volume for RC2901-731 section and < 0.1% of total volume for SO161-
135 35 section), while low gas hydrate concentrations (<4% of total volume in both sections) are in
136 correspondence with high free gas concentrations (up to 1.1 % of total volume for SO161-35 and up
137 to 0.3% of total volume for RC2901-731 sections; see Fig. 3).

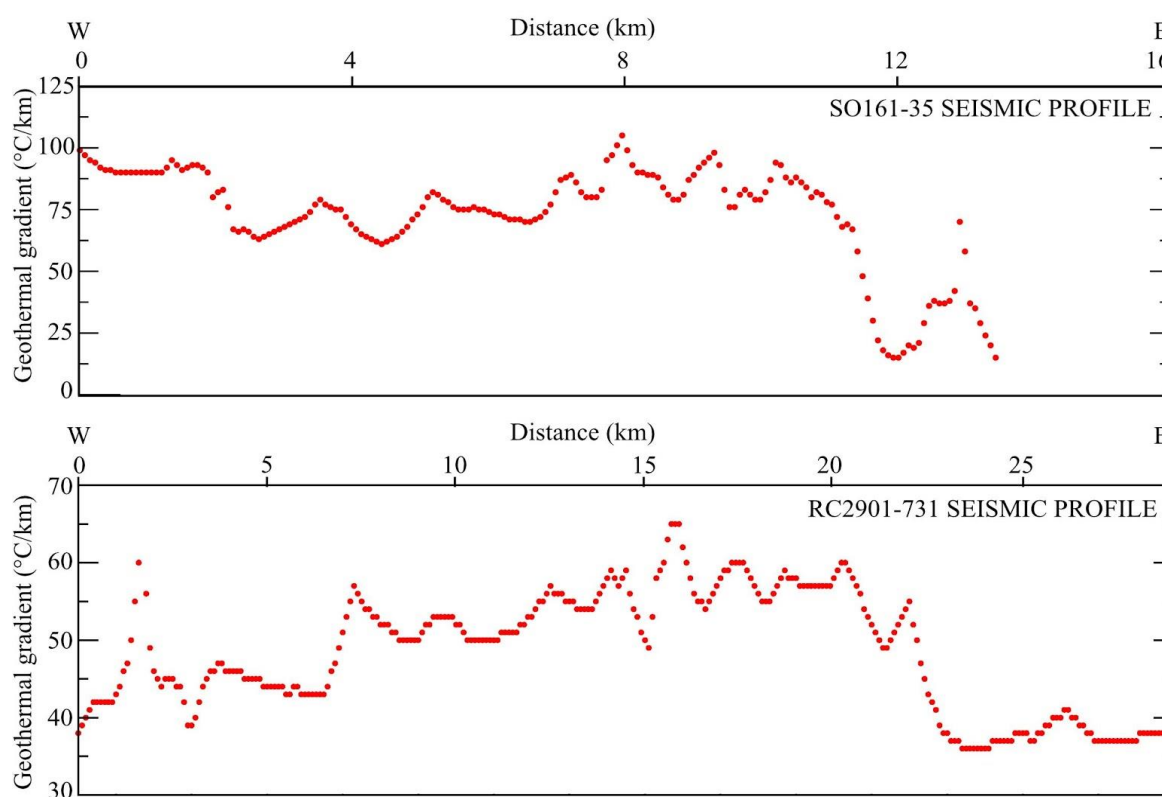


138

139 **Figure 3.** Line drawing sections with superimposed gas phase (gas hydrate and free gas)
 140 concentration models. Top three panels: SO161-35 seismic profile. Bottom three panels: RC2901-731
 141 seismic profile. Above each sections are reported gas hydrate (black diamonds) and free gas (blue
 142 diamonds) concentration values. Dashed black and blue lines show average values.

143 A variable geothermal gradient across sections was obtained. However, a recognisable higher
 144 geothermal gradient was identified across SO161-35 section (ranging from 60 to 110 °C/km), while
 145 lower geothermal gradient across RC2901-731 section was observed (ranging from 35 to 65 °C/km).
 146 The seismic and line drawing sections (Figs. 2 and 3) underline that the lowest geothermal values are

147 located upwards in correspondence with the submarine canyon for SO161-35 section (see Fig. 3 above
 148 section at 12 km of distance) and the normal fault for RC2901-731 section (see Fig. 2 below section
 149 at 22 km of distance).



150

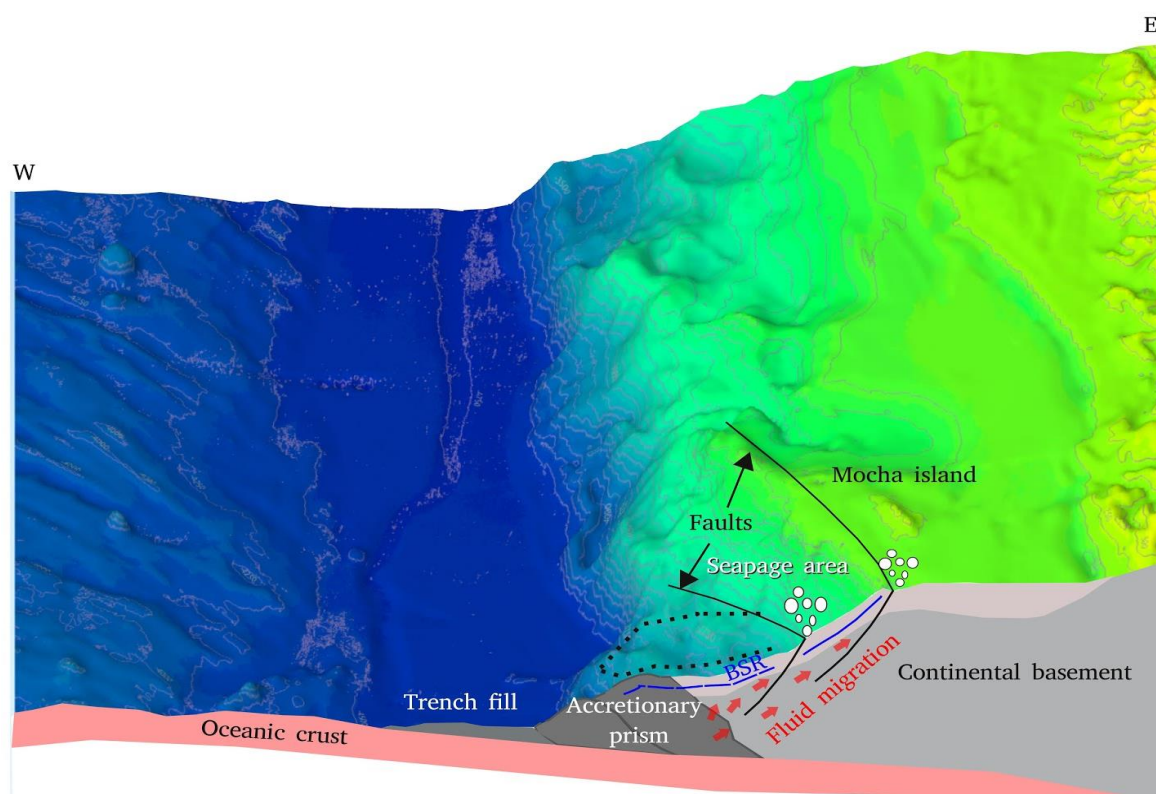
151 **Figure 4.** Estimated geothermal gradients. Top: SO161-35 seismic profile. Below: RC2901-731 seismic
 152 profile.

153 4. Discussion

154 Faults, fractures and folding affecting the shallow sediments in both sections are related to an
 155 active domain. In fact, Mocha island is characterised by high seismicity and the uplifting process
 156 started during Quaternary [18]. The SO161-35 seismic profile is located approximately 12 km
 157 southern Mocha island and shows a strong and continuous BSR, while SO161-731 seismic profile,
 158 distant from Mocha island approximately 60 km south, evidences a discontinuous and locally strong
 159 BSR. Moreover, a lateral variable BSR depth close to Mocha island (SO161-35 section) was identified,
 160 while along RC2901-731 only a slight variation in the BSR depth was recognisable. The BSR seismic
 161 character and its depth variability can be related to the gas phase concentrations and the geothermal
 162 gradient distribution. Regarding BSR seismic character, several studies argue that strong and
 163 continuous BSRs are related to significative free gas concentrations and strong vertical velocity
 164 variations [8,34,35]. In our case, across SO161-35 seismic profile the highest free gas concentrations
 165 up to 1.1% of total volume (associated to the lowest velocity equal to 1260 m/s) are related to strong
 166 vertical velocity variation of 640 m/s, which is the velocity difference between gas hydrate and free
 167 gas velocity layers. On the other hand, faraway from Mocha island (RC2901-731 seismic profile), the
 168 lowest velocity below BSR increases to 1450 m/s and the difference between gas hydrate and free gas
 169 velocities decreases to 400 m/s with respect to the seismic velocity determined in proximity of the
 170 Mocha island. The variable depth of the BSR along the SO161-35 section can be explained by a
 171 variable geothermal gradient, in which high geothermal gradient values ranging from 60 to 110
 172 °C/km, while a constant BSR depth along the RC2901-731 section could be asociated to low
 173 geothermal gradient values ranging from 35 to 65 °C/km, characterized by a slightly lateral variation.

174 Along the RC2901-731 line, the discontinuous and locally strong seismic character of the BSR can be
 175 related with lateral folding presence, in which the gas hydrate and the free gas appear trapped by
 176 least across faults and fractures and are highly concentrated at the folding crest. In fact, along this
 177 section, areas characterized by high/low velocity above/below the BSR in correspondence to small
 178 folding and faults are detected (see RC2901-731 seismic profile in Figs. 2 and 3). Our result is in
 179 agreement with several authors that have reported anticlinal structures as structural traps for fluid
 180 storing associated to gas hydrate occurrences [12,36-38].

181 Higher geothermal gradient values were obtained close to Mocha island with average value
 182 equal to 85 °C/km against lower geothermal gradient values far off Mocha island with average value
 183 equal to 50 °C/km. These results are in agreement with anomalous heat flows reported by [15] in the
 184 same area. The former authors argue that the high heat flow variability would be related to ancient
 185 sliding processes, in which the headwall slide constitutes a fluid advection zone altering the
 186 geothermal gradient at the present. In addition, some authors have proposed this area as a hydrated
 187 and/or fluid saturated forearc region [39]. In this context, the fluid supply from deep including gas
 188 can be canalised by faults and fractures (Fig. 5) and reaches the hydrate stability zone altering the
 189 thermal state giving place to high geothermal gradients as reported in this study. Decreased
 190 geothermal gradient faraway from Mocha island is associated with the regional geothermal gradient
 191 [15,26,27].



192
 193 **Figure 5.** Schematic diagram of SO161-35 seismic profile located close to 38°30'S (see Fig. 1),
 194 explaining fluid migration processes close to the Mocha island. Faults are reported by [17,18]. Dashed
 195 line shows part of the ancient sliding reported by [40].

196 High gas hydrate concentrations up to 20% of total volume are reported in both sections, but the
 197 highest free gas concentrations up to 1.1% of total volume are located near to the Mocha island
 198 (SO161-35 seismic profile), while the lowest free gas concentrations up to 0.3% of total volume are
 199 found faraway Mocha island (across RC2901-731 section). In both sections, the highest gas hydrate
 200 concentration can be explained as follows: a) high fluid supply from deep zones that can favour gas
 201 hydrate formation, as suggested by several authors [15,38] and b) overestimates by compaction due
 202 to deformation processes. On the other hand, the highest free gas concentration located near the

203 Mocha island would be related to the gas hydrate dissociation associated to past sliding processes
204 reported by [40] or free gas stored below an impermeable gas hydrate layer (see Fig. 5), while the
205 lowest free gas concentrations across RC2901-731 seismic line can be explained by lower fluid supply
206 from deep zones and high fluid escape rates preventing free gas storing. These fluid escapes are
207 canalised by faults and fractures affecting seafloor and releasing gas like seeps.

208 Finally, considering high gas hydrate (average 7.5 % of total volume) and free gas concentrations
209 (0.4 % of total volume) reported in this study, we conclude that close to the Mocha island gas hydrate
210 dissociation processes occurring in the past and, potentially, in the present can constitute the main
211 seepage supply source along this part of the Chilean margin.

212

213 **Author Contributions:** All authors were involved in the data processing and preparation process.
214 All authors were involved in the discussion and revision process with section leads as follows: Iván
215 Vargas-Cordero (Section 1, Section 2, Section 3 and Section 4), Umberta Tinivella (Section 2, Section
216 3 and Section 4), Lucia Villar-Muñoz and Joaquim P. Bento (Section 3 and 4).

217 **Funding:** This research was partially funded by Conicyt, Chile (Fondecyt program), project number
218 11140216.

219 **Acknowledgments:** The authors are very grateful to Joyce Alsop for the seismic data provided at
220 Lamont Doherty Earth Laboratory, USA (LDEO) and V. Damm for the seismic data provided at
221 Federal Institute for Geosciences and Natural Resources, Germany (BGR). We are grateful to
222 CONICYT (Fondecyt de Iniciación N°11140216), which partially supported this work.ts).

223 **Conflicts of Interest:** The authors declare no conflict of interest.

224 References

- 225 1. Kvenvolden, K. A. Gas hydrates-geological perspective and global change. *Reviews of*
226 *geophysics* 1993, 31(2), 173-187.
- 227 2. Bouriak, S.; Vanneste, M.; Saoutkine, A. Inferred gas hydrates and clay diapirs near the Storegga
228 Slide on the southern edge of the Vøring Plateau, offshore Norway. *Marine Geology* 2000, 163(1-
229 4), 125-148.
- 230 3. Bünz, S.; Mienert, J.; Berndt, C. Geological controls on the Storegga gas-hydrate system of the
231 mid-Norwegian continental margin. *Earth and Planetary Science Letters* 2003, 209(3-4), 291-307.
- 232 4. Sultan, N.; Cochonat, P.; Canals, M.; Cattaneo, A.; Dennielou, B.; Haflidason, H.; Urgeles, R.
233 Triggering mechanisms of slope instability processes and sediment failures on continental
234 margins: a geotechnical approach. *Marine Geology* 2004, 213(1-4), 291-321.
- 235 5. Berndt, C.; Mienert, J.; Vanneste, M.; Bünz, S. Gas hydrate dissociation and sea-floor collapse in
236 the wake of the Storegga Slide, Norway. In *Norwegian Petroleum Society Special Publications*,
237 2005, 12, 285-292.
- 238 6. Horozal, S.; Bahk, J. J.; Urgeles, R.; Kim, G. Y.; Cukur, D.; Kim, S. P.; Kim, J. H. Mapping gas
239 hydrate and fluid flow indicators and modelling gas hydrate stability zone (GHSZ) in the
240 Ulleung Basin, East (Japan) Sea: Potential linkage between the occurrence of mass failures and
241 gas hydrate dissociation. *Marine and Petroleum Geology* 2017, 80, 171-191.
- 242 7. Bangs, N. L.; Sawyer, D. S.; Golovchenko, X. Free gas at the base of the gas hydrate zone in the
243 vicinity of the Chile triple junction. *Geology*. 1993, 21(10), 905-908.
- 244 8. Brown, K. M.; Bangs, N. L.; Froelich, P. N.; Kvenvolden, K. A. The nature, distribution, and
245 origin of gas hydrate in the Chile Triple Junction region. *Earth and Planetary Science Letters*
246 1996, 139(3-4), 471-483.
- 247 9. Morales, G. Methane hydrates in the Chilean continental margin. *Electronic Journal of*
248 *Biotechnology* 2003, 6(2), 80-84.
- 249 10. Rodrigo, C.; González-Fernández, A.; Vera, E. Variability of the bottom-simulating reflector
250 (BSR) and its association with tectonic structures in the Chilean margin between Arauco Gulf
251 (37°S) and Valdivia (40°S). *Mar. Geophys. Res.* 2009, 30, 1-19.

- 252 11. Vargas-Cordero, I.; Tinivella, U.; Accaino, F.; Loreto, M. F.; Fanucci, F. Thermal state and
253 concentration of gas hydrate and free gas of Coyhaique, Chilean Margin (44° 30' S). *Marine and*
254 *Petroleum Geology* 2010, 27(5), 1148-1156.
- 255 12. Vargas-Cordero, I.; Tinivella, U.; Accaino, F.; Loreto, M. F.; Fanucci, F.; Reichert, C. Analyses of
256 bottom simulating reflections offshore Arauco and Coyhaique (Chile). *Geo-Marine Letters* 2010,
257 30(3-4), 271-281.
- 258 13. Vargas-Cordero, I.; Tinivella, U.; Villar-Muñoz, L.; Giustiniani, M. Gas hydrate and free gas
259 estimation from seismic analysis offshore Chiloé island (Chile). *Andean Geology* 2016, 43(3),
260 263-274.
- 261 14. Vargas-Cordero, I.; Umberta, T.; Villar-Muñoz, L. Gas Hydrate and Free Gas Concentrations in
262 Two Sites inside the Chilean Margin (Itata and Valdivia Offshores). *Energies* 2017, 10(12), 2154,
263 doi:10.3390/en10122154.
- 264 15. Villar-Muñoz, L.; Behrmann, J. H.; Diaz-Naveas, J.; Klaeschen, D.; Karstens, J. Heat flow in the
265 southern Chile forearc controlled by large-scale tectonic processes. *Geo-Marine Letters* 2014,
266 34(2-3), 185-198.
- 267 16. Villar-Muñoz, L.; Berto, J. P.; Klaeschen, D.; Tinivella, U.; Vargas-Cordero, I.; Behrmann, J. H. A
268 first estimation of gas hydrates offshore Patagonia (Chile). *Marine and Petroleum Geology* 2018,
269 96, 232-239. doi: 10.1016/j.marpetgeo.2018.06.002.
- 270 17. Melnick, D.; Echtler, H. P. Inversion of forearc basins in south central Chile caused by rapid
271 glacial age trench fill, *Geology* 2006, 34(9), 709-712.
- 272 18. Melnick, D.; Bookhagen B.; Echtler, H.; Strecker M. Coastal deformation and great subduction
273 earthquakes, Isla Santa Maria, Chile(37°S), *Geol. Soc. Am. Bull.* 2006, 118(11), 1463-1480,
274 doi:10.1130/B25865.1.
- 275 19. Jessen, G. L.; Pantoja, S.; Gutierrez, M. A.; Quinones, R. A.; Gonzalez, R. R.; Sellanes, J.; Hinrichs,
276 K. U. Methane in shallow cold seeps at Mocha Island off central Chile. *Continental Shelf*
277 *Research* 2011, 31(6), 574-581.
- 278 20. Sellanes, J.; Zapata-Hernández, G.; Pantoja, S.; Jessen, G. L. Chemosynthetic trophic support for
279 the benthic community at an intertidal cold seep site at Mocha Island off central Chile. *Estuarine,*
280 *Coastal and Shelf Science* 2011, 95(4), 431-439.
- 281 21. Stuardo, J.; Valdovinos, C. A new bathyal Calyptogena from the coast of central Chile (Bivalvia:
282 Vesicomidae). *Venus* 1988, 47, 241-250.
- 283 22. Tinivella, U.; Loreto, M. F.; Accaino, F. Regional versus detailed velocity analysis to quantify
284 hydrate and free gas in marine sediments: the South Shetland Margin case study. *Geological*
285 *Society, London, Special Publications* 2009, 319(1), 103-119.
- 286 23. Cohen, J.K.; Stockwell, J.W. CWP/SU: Seismic Unix Release 4.0: A free Package for Seismic
287 Research and Processing. Center for Wave Phenomena, Colorado School of Mines: Golden, CO,
288 USA. 2008, 1-153.
- 289 24. Liu, Z.; Bleistein, N. Migration velocity analysis: Theory and an iterative algorithm. *Geophysics*
290 1995, 60, 142-153.
- 291 25. Yilmaz, O. *Seismic Data Analysis: Processing, Inversion and Interpretation of Seismic Data*. 2nd
292 Edition. Society of Exploration Geophysicists, Oklahoma. 2001, 2027.
- 293 26. Grevemeyer, I.; Diaz-Naveas, J.L.; Ranero, C.R.; Villinger, H.W. Ocean Drilling Program
294 Scientific Party. Heat Flow over the descending Nazca plate in Central Chile, 32° S to 41° S:
295 Observations from ODP Leg 202 and the occurrence of natural gas hydrates. *Earth Planet. Sci.*
296 *Lett.* 2003, 213, 285-298.
- 297 27. Grevemeyer, I.; Villinger, H. Gas hydrate stability and the assessment of heat flow through
298 continental margins. *Geophys. J. Int.* 2001, 145, 647-660.
- 299 28. Dickens, G.R.; Quinby-Hunt, M.S. Methane hydrate stability in seawater. *Geophys. Res. Lett.*
300 1994, 21, 2115-2118.
- 301 29. Chand, S.; Minshull, T.A.; Gei, D.; Carcione, J.M. Elastic velocity models for gas hydrate bearing
302 sediments a comparison. *Geophysical Journal International* 2004, 159, 573-590.

- 303 30. Tinivella, U. The seismic response to overpressure versus gas 638 hydrate and free gas
304 concentration. *Journal Seismic Exploration* 2002, 11, 283-305.
- 305 31. Tinivella, U.; Carcione, J.M. Estimation of gas hydrate concentration and free gas saturation from
306 log and seismic data. *The Leading Edge* 2001, 20, 200-203.
- 307 32. Hamilton, E.L. Sound velocity gradients in marine sediments. *J. Acoust. Soc. Am.* 1979, 65, 909-
308 922.
- 309 33. Tinivella, U. A method for estimating gas hydrate and free gas concentrations in marine
310 sediments. *Boll. Geofis. Teor. Appl.* 1999, 40, 19-30.
- 311 34. Hyndman R.D.; Spence G.D. A seismic study of methane hydrate marine bottom simulating
312 reflectors, *J. geophys. Res.* 1992, 97, 6683-6698.
- 313 35. Hovland, M.; Gallagher, J. W.; Clennell, M. B.; Lekvam, K. Gas hydrate and free gas volumes in
314 marine sediments: Example from the Niger Delta front. *Marine and Petroleum Geology* 1997,
315 14(3), 245-255.
- 316 36. Inks, T.; Lee, M.; Agena, W.; Taylor, D.; Collett, T.; Hunter, T.; Zyrianova, M. Seismic prospecting
317 for gas hydrate and associated free gas prospects in the Milne Point area of northern Alaska. In:
318 Collett, T., Johnson, A., Knapp, C., Boswell, R. (Eds.), *Natural Gas Hydrates – Energy Resource
319 Potential and Associated Hazards*. AAPG Memoir, 2009, 89.
- 320 37. Loreto, M.F.; Tinivella, U. Gas hydrate versus geological features: The South Shetland case
321 study. *Mar. Pet.Geol.* 2012, 36, 164-171.
- 322 38. Boswell, R.; Rose, K.; Collett, T. S.; Lee, M.; Winters, W.; Lewis, K. A.; Agena, W. Geologic
323 controls on gas hydrate occurrence in the Mount Elbert prospect, Alaska North Slope. *Marine
324 and Petroleum Geology* 2011, 28(2), 589-607.
- 325 39. Haberland, C.; Rietbrock, A.; Lange, D.; Bataille, K.; Dahm, T. Structure of the seismogenic zone
326 of the south central Chilean margin revealed by local earthquake traveltime tomography.
327 *Journal of Geophysical Research: Solid Earth* 2009, 114(B1).
- 328 40. Geersen, J.; Voelker, D.; Behrmann, J. H.; Reichert, C.; Krastel, S. Pleistocene giant slope failures
329 offshore Arauco Peninsula, Southern Chile. *J Geol Soc.* 2011, 168, 1237-1248.



© 2018 by the authors. Submitted for possible open access publication under the terms and conditions of the Creative Commons Attribution (CC BY) license

332 (<http://creativecommons.org/licenses/by/4.0/>).